arXiv:nucl-th/9803016v1 5 Mar 1998

Using inverse scattering methods to study inter-nucleus potentials

R S Mackintosh† and S G Cooper†

† Physics Department, Open University, Milton Keynes MK7 6AA, UK

Abstract. It is now straightforward to carry out S-matrix to potential inversion over a very wide range of energies and for a wide range of projectile-target combinations. Inversion is possible in many cases involving spin. IP inversion also permits direct scattering data-to-potential inversion and furnishes powerful tools for the phenomenological analysis of nuclear scattering. The resulting single particle potentials exhibit various generic properties which challenge fundamental reaction theories as well as yield information on densities, provide input for reaction calculations. S-matrix to potential inversion is also a powerful tool for directly investigating theoretical processes which contribute to inter-nuclear potentials. Various studies have given insight into contributions to the dynamic polarisation potential (DPP) due to breakup processes and due to collective and reaction channel coupling and have also illuminated the role played by exchange processes in leading to non-locality and parity dependence of the potentials. A case study involving d + ^{4}He is a model for ways in which inversion applied jointly to theory and experiment might illuminate the scattering of exotic nuclei.

PACS numbers: 25.10.+s, 25.60.Bx, 25.45.-z, 24.10.-i, 24.70.+s

Short title: Using inverse scattering methods

February 9, 2008

1. Introduction

There now exists a highly developed and indefinitely generalisable 'inversion' technique which makes it straightforward to carry out S-matrix to potential inversion over a very wide range of energies and for a wide range of projectile-target combinations. This is the 'iterative perturbative', IP, method. Inversion by means of the IP method offers many possibilities for increasing our physical understanding of nuclear scattering and inter-nuclear potentials, both for stable and unstable nuclei. Here we support this claim by: (1) briefly indicating the underlying principles of IP inversion; (2) giving an overview of the range of applicability of the IP method — this amounts to specifying what we mean by 'inversion', an increasingly general concept; (3) indicating with typical examples the two basic ways it can be applied, i.e. to theoretical and empirical S_l; and, (4) presenting a case study to show how a joint study of theoretical and empirical S_l brings potential models centre stage as we fit data that had never been fitted and at the same time evaluate a theoretical model for which there had been no satisfactory evaluation. In doing this, we show the power of potential models once freed of historical limitations. The case study concerns d + ^{4}He scattering. The deuteron is, of course, the archetypal weakly bound projectile and the d + ^{4}He system is one where there is some chance of a fully microscopic description, and also where there is a large amount of data. It is therefore an ideal testing ground for some of the physics relating to more exotic highly polarizable nuclei.

To date, most of the applications have not been to nuclei far from stability; we draw attention to the exceptions. There is considerable potential for applications to exotic nuclei and there will be many applications that we are unaware of. The method is implemented in a very general code IMAGO [1] which we are making portable.

2. IP inversion; range of applicability

Historically, fixed-l inversion refers to the formal determination of the potential $V(r)$ which leads via Schrödinger's equation to S_l for some fixed l and all energies $E \to \infty$; fixed energy inversion is the determination of $V(r)$ from S_l for all l at some fixed energy. Practical versions of formal methods [2] for fixed-l and fixed energy inversion that can handle, for example, finite ranges of energy or of l have disadvantages and progress toward practical means of treating spin has been slow. Moreover, S_l which are imprecise or defined over small l ranges are difficult to handle, so the number of applications yielding real physical insight has been small.

A less formal method, iterative perturbative (IP) inversion, has been developed [3, 4, 5, 6, 7]. IP inversion is very general and is readily extended to include spin. It can, moreover, give meaningful results with S_l given over small ranges of l and also for S_l which are imprecisely determined. This last point turns out to be a crucial advantage in many situations, particularly when experimental data is fitted.

The IP method has been described a number of times [3, 4, 5, 6, 7, 8], so we do no more than briefly outline the underlying concepts. The key idea is iteratively to correct a potential $V(r)$ by adding terms

$$V(r) \to V(r) + \sum c_i v_i(r) \tag{1}$$

where $v_i(r)$ are members of a suitable set of 'basis functions' and c_i are amplitudes derived from linear equations arising from the response, assumed linear, of the elastic

scattering S-matrix to small changes δV in the potential:

$$\delta S_l = -\frac{\mathrm{i}m}{\hbar^2 k}\int_0^\infty (u_l(r))^2 \delta V(r)\mathrm{d}r. \tag{2}$$

In Equation 2, the radial wavefunction for angular momentum l is normalised according to $u_l(r) \rightarrow I_l(r) - S_l O_l(r)$ where I_l and O_l are the incoming and outgoing Coulomb wavefunctions. The notation is simplified: $V(r)$ stands for real and imaginary, central and spin-orbit terms which can be expanded in different bases; for the cases where spin and many energies are treated see the papers cited above.

IP inversion is indefinitely generalisable. The possibilities include:

i. Fixed energy inversion For one energy and for finite set of l, $S_l \rightarrow V(r)$. The problem at low energies is that there are too few partial waves to yield a usefully defined potential.

ii. Mixed case (energy bite) inversion The problem noted for fixed energy inversion can be solved where (as is often the case) one has available the set S_l over a range of energies ('energy bite'). For a narrow bite, this is tantamount to including $\mathrm{d}S_l/\mathrm{d}E$ as input information into the inversion.

iii. Energy dependent inversion Often, one expects the potential, particularly the imaginary parts, to vary over the relevant energy range. In this case, IP inversion can be extended to determine directly an energy dependent potential. In published cases [9], this is limited to the factored form $f(E)V(r)$ for each component, but this limitation will be lifted in the future.

iv. Inversion to fit bound state and resonance energies Bound state and resonance energies can be included in the input information for the inversion.

v. Direct data to potential inversion This new development is discussed in Section 3.2.3.

IP inversion can be applied to spinless projectiles, $S_l \rightarrow V(r)$, or spin 1/2 projectiles, $S_{lj} \rightarrow V(r) + \mathbf{l}\cdot\sigma V_{ls}(r)$, where V is complex if $|S| < 1$. Inversion for spin 1 and spin 3/2 projectiles leading to vector spin-orbit potentials has been carried out and the generalisation to tensor forces is under development.

For the case of identical bosons, one can determine potentials given S_l for even l only. For many pairs of interacting nuclei, it is possible to determine Wigner and Majorana terms for each component, symbolically: $V_{\mathrm{W}}(r) + (-1)^l V_{\mathrm{M}}(r)$. Both theory and experiment make Majorana components obligatory in many cases. Indeed, it often emerges that inverting some given S_l presents a choice between oscillatory pure Wigner potentials and relatively smooth potentials which having Majorana components. In some cases, highly oscillatory l-independent potentials which are S_l-equivalent to explicitly parity dependent phenomenological potentials have been determined.

3. How inversion can be applied.

Theory and experiment both provide S_l, and it is often fruitful to compare $V(r)$ inverted from both sources for the same scattering situation. Examples are p + ^{4}He, described in Ref. [9], and d + ^{4}He, described in Section 4. One key point is that the best basic theory (typically RGM) cannot closely fit the data. But many qualitative

features can be extracted by inversion of RGM S_l, see Section 3.1.3. These can be compared with the same features extracted from experimental data by the use of inversion techniques, often the *only* way of extracting these properties.

3.1. Analysis of theoretical S-matrix.

3.1.1. Dynamic polarization potentials A local representation of the dynamic polarization potential, DPP, arising from the coupling to specific channels, follows immediately by inverting the elastic S_l given by CC, CRC, CDCC, adiabatic model etc. and subtracting the bare potential. Of relevance to halo nuclei is the fact that the real part of the DPP arising from the breakup of loosely bound projectiles tends to have [10] a characteristic pattern of repulsion in the far surface and attraction at smaller radii. The geometric properties of the real potential are thereby modified and so therefore are deductions concerning the nuclear size.

3.1.2. Local equivalent potentials Often, the most direct and efficient means of finding the local equivalent of a non-local potential is inversion. In particular, we have determined [11] the energy dependent local potential that represents the Perey Buck non-local potential and verified that its energy dependence agrees well with that derived from RGM (see below) and also the phenomenological energy dependence.

3.1.3. Potentials from microscopic theory Certain theories of nuclear reactions do not naturally yield a local potential model, yet potentials still provide an essential link to phenomenology. For *ab initio* calculations of scattering involving light nuclei, the best existing model is probably the resonating group model, RGM. Agreement with experiment is qualitative as a result of the necessary use of schematic interactions and the omission of important configurations. Nevertheless, the fact that RGM does yield qualitatively correct features emerges when one determines potentials from RGM S_{lj}. Recent RGM studies include: Ref. [12] which assesses the Majorana terms for helion and alpha scattering from nuclei as heavy as ^{16}O; Ref. [13] which determines the Majorana term for the nucleon-nucleus potential for nuclei as heavy as ^{40}Ca. Both papers analyse the contribution of specific exchange or coupling terms in the RGM kernel to the strength and energy dependence of specific Wigner or Majorana terms in the inter-nucleus potential. The agreement between RGM and experiment for p + ^{4}He [9] is mentioned in Section 3.2.2.

3.2. Inversion of S-matrix derived from experimental data

3.2.1. Two-step phenomenology, discrete energies As an alternative to standard model-independent optical-model phenomenology, one can fit the elastic scattering differential cross-section with an S-matrix function $S(l)$ and then invert. The second step is by far the more straightforward. Concerning the first step, the good news is that phenomenology is liberated from prejudices concerning the form of the potential; the bad news is the immense range of ambiguities which emerges. What was originally impossible to fit precisely becomes all too easy to fit. In fact, the realization of just how profound the ambiguities are, even at the level of essentially perfect fits, is a clear lesson which emerges. One must therefore judiciously reinstate some prejudices, such as continuity with energy, and, most usefully, a relationship between the behaviour of $|S(l)|$ (and to a lesser extent $\arg S(l)$) and the same quantities derived from the

static approximation Glauber model. This has been done for ^{16}O + ^{16}O [14], ^{12}C + ^{12}C [15], and ^{11}Li scattering from ^{12}C and ^{28}Si [16]. Referring to the figures in Ref. [16], one sees that it is indeed all too easy to get essentially perfect fits to the data, radical ambiguities existing even at the S_l level. We argue in Ref. [16] that our least unreasonable fit to ^{11}Li elastic scattering data corresponds to a potential with a long tail in the real potential. This feature cannot be explained on the basis of current theories of ^{11}Li. Similar potentials for ^{11}Li + ^{12}C were found by Mermaz [17] by quite different means. There was no evidence for such a tail in the non-halo ^{11}C + ^{12}C case. It is widely believed that these fits reflect faulty data and that new data will be fitted by a potential more in line with current theory. We keenly await the arrival of such new data, preferably for as wide as possible an angular range, and for as many energies as possible. The full information content of such data can be exploited. Since the ^{11}Li work [16], we have learned new ways to incorporate information from many energies, see Section 3.2.3.

3.2.2. Two-step phenomenology, parameterised $S_{lj}(E)$ The ambiguity problem is much reduced when data at a series of energies is fitted with a functional form $S_{lj}(E)$ to which one applies 'mixed case' or energy dependent inversion. Such forms of $S_{lj}(E)$ for few nucleon systems are typically R-matrix or effective range fits. There are limits to the energy over which smooth $S_{lj}(E)$ exist, but one can also incorporate $S_{lj}(E_i)$ for discrete energies E_i (one can also fit just the discrete $S_{lj}(E_i)$ blurring the distinction from the previous category.) For p + ^{4}He scattering, a Majorana term, falling quite rapidly with energy, emerges, in agreement with that found by inverting RGM S_{lj}. The energy dependence of the Wigner term, largely due to knock-on exchange, is consistent with nucleon-nucleus phenomenology [9].

3.2.3. Direct observable to potential inversion Recently, a generalisation of the IP method for direct observable to potential inversion has been developed [5, 7]. The key idea is that the linear equations by which amplitudes c_i are determined at each iteration arise from the minimisation of the goodness of fit quantity χ^2:

$$\frac{\partial \chi^2}{\partial c_i} = 2\sum_{k,l}\left[\frac{\sigma_k - \sigma_k^{\rm in}}{(\Delta\sigma_k^{\rm in})^2}\right]\frac{\partial \sigma_k}{\partial S_l(E_k)}\frac{\partial S_l(E_k)}{\partial c_i} + 2\sum_{n,k,l}\left[\frac{P_{kn} - P_{kn}^{\rm in}}{(\Delta P_{kn}^{\rm in})^2}\right]\frac{\partial P_{kn}}{\partial S_l(E_k)}\frac{\partial S_l(E_k)}{\partial c_i} \quad (3)$$

where $\sigma_k^{\rm in}$ and $P_{kn}^{\rm in}$ are the input experimental values of cross sections and analyzing powers respectively (n indexing the spin related observables for spin 1 systems), and

$$\chi^2 = \sum_{k=1}^{N}\left(\frac{\sigma_k - \sigma_k^{\rm in}}{\Delta\sigma_k^{\rm in}}\right)^2 + \sum_n \sum_{k=1}^{M}\left(\frac{P_{kn} - P_{kn}^{\rm in}}{\Delta P_{kn}^{\rm in}}\right)^2. \quad (4)$$

Since we are fitting data for many energies at once, the index k indicates the energy as well as angle. The power of this approach will be evident from the d + ^{4}He case study described below, but we note that it has yielded the best phenomenological description of p + ^{16}O scattering to date [7].

4. Experiment and theory of d + ^{4}He scattering

Here we bring together RGM theory, the adiabatic model of breakup and a large compilation [20] of experimental data to present an emerging picture of d + ^{4}He scattering. This is work in progress with many issues to be settled.

4.1. *Inversion analysis of RGM calculations*

The RGM S_{lj} are from the multi-configuration RGM (MCRGM) study by Kanada *et al* [21], hereafter KKST, of elastic scattering of deuterons by ^{4}He. Up to 8 pseudo-states in the deuteron wavefunction were coupled to the elastic scattering to represent S-wave breakup. A phenomenological imaginary potential was included in order to represent the effects of omitted open channels. The N-N interaction was somewhat schematic in line with the demands of RGM calculations of this complexity. In particular, there was a spin-orbit but no tensor NN force. Both the ^{4}He nucleus and the deuteron were pure S-wave and there was no breakup into deuteron D-states. In Ref. [18] we discussed the inversion of the KKST S_{lj} for deuteron laboratory energies of 29.4 and 56 MeV and presented complex potentials with spin-orbit components, plus Majorana terms for each component.

It follows from Figures 1 and 2 of Ref. [18] that the real, Wigner, central part of the potentials varied in a reasonable way with energy. At 29.4 MeV, the volume integral per nucleon pair was $J_{\mathrm{R}} = 499.72$ MeV fm^3 and the rms radius was 2.905 fm (c.f. Section 4.3). The real Wigner spin-orbit potential was unusual in form, having a deep minimum at the nuclear centre, but was reasonable in magnitude. It is relevant for what follows below that this shape seemed to be well determined and was almost identical for both energies and very similar to the corresponding term determined from S_{lj} for the no-breakup RGM calculations of Lemere *et al* [22]. We note two provisos concerning the spin-orbit form: the spin-orbit potential is not determined for $r <$ the turning point for P-waves, ~ 0.5 fm, so the inner cusp is just a smooth continuation of the potential further out. Secondly, tensor forces are omitted; while there are no off-diagonal matrix elements generated by the RGM calculations, the vector potential might well be mocking up effects which are of tensor nature [18]. Unlike the real spin-orbit terms, other components were different at the two energies, probably because of the marked increase with energy of flux into reaction channels.

The MCRGM of KKST gave qualitative fits to experiment. The question then arises: how well do these calculations describe d + ^{4}He elastic scattering? It could be claimed that the fits are what one might expect of any potential with correct overall strength and radius and a freely fitted additional imaginary term. We give an account below of the extent to which KKST MCRGM calculations do lead to a potential model consistent with good description of d + ^{4}He elastic scattering.

4.2. *D-wave breakup*

How important is the omission of D-wave breakup in the RGM calculations? To estimate this, we performed adiabatic model breakup calculations[23] using the code Adia [24]. Inversion of S_l (spin was ignored) led to the conclusion that as far as the real potential was concerned, the contribution of S-wave breakup is largely confined to the central region, $r \leq 1.5$ fm, where it generates a considerable extra attraction, a feature also found in RGM by Kukulin *et al* [25]. On the other hand, D-wave breakup induces extra attraction over a wide radial range, but repulsion in the surface region. The effect is therefore to reduce the rms radius of the real potential.

The effect on the imaginary central potential of adding D-wave breakup is similar to the effect on the real part. Instead of being confined to the centre of the nucleus, as it is for S-wave breakup, we find added absorption at all radii within the nucleus. However, according to the adiabatic model, one characteristic effect of adding deuteron

breakup is the generation of a very deep absorptive region near the nuclear centre. Such a deep feature is not found in the MCRGM results, Section 4.1, nor, at lower energies at least, empirically, Section 4.3. It remains to be studied whether it is the adiabatic assumption or the neglect of exchange which is responsible for the difference. Not only does MCRGM predict a less absorptive region near $r = 0$, but sometimes local emissivity, a phenomenon associated with strong non-local effects which are often very different from the Perey effect. We conclude that D-state breakup is not ignorable in d + ^{4}He scattering. The contributions to the local d + ^{4}He potential induced by breakup are generally consistent with generic effects [10] for heavy target nuclei. The fact that S-wave breakup induces attraction plus absorption only at the nuclear centre while D-wave breakup induces a polarization potential for all r is due in general terms to the fact that the intermediate state partial wave l can change by ± 2 in the latter case, but a more detailed explanation would be welcome.

4.3. Fitting experimental data: d + ^{4}He elastic scattering ≤ 11.5 *MeV*

There is much experimental data for d + ^{4}He elastic scattering. It has been carefully assembled and evaluated by Kuznetsova and Kukulin [26] who also present a phase shift analysis, PSA. The serious problems arising with such analyses motivate work in preparation, see Ref. [27], in which this data is fitted in the course of demonstrating how inversion leads to a solution of the phase shift analysis problem. Here, our concern is to exploit potential models to confront experiment with RGM. Of the many available data sets we have fitted two: one (set 'J') comprises the angular distributions and vector analysing powers of Jenny *et al* [28] at 5 deuteron laboratory energies between 6.24 MeV and 10 MeV. The second (set 'SG') combines the differential cross sections at 19 energies between 2.935 and 11.475 MeV [29] and vector analysing powers at 12 energies between 3.0 and 11.5 MeV [30], 539 data in all. As in Ref. [27], the differential cross sections and analysing powers of one of the two (J or SG) data sets for all energies are fitted to a single potential (which we designate respectively as the J or SG potential) using the direct data-to-potential form of IP inversion described in Section 3.2.3. We have not exploited the possibility [9] of determining a fully energy dependent potential, the real components all being energy independent. However, the imaginary components are energy dependent. When fitting the SG data, all imaginary components are assumed to be zero below $E_{\rm th}$, $E_{\rm th}$ being the inelastic threshold energy. For both J and SG data, all imaginary components are proportional to $(E - E_{\rm th})$ above $E_{\rm th}$. Tensor observables are not fitted and we include no representation of tensor forces, these being understood to have a small effect on vector analysing power. The starting potential for the IP procedure was that described in Section 4.1 as fitting the 29.4 MeV KKST S_{lj}. Although it is possible to include the S-wave bound state energy of -1.472 MeV in the inversion input data, mostly we did not do this. Instead, the bound state energy was monitored to verify the consistency of the inversion. The possible dependence of the results on the starting potential must be borne in mind in the following discussion.

Remarkably, the inversion process† converged very rapidly to a potential that was rather close to the starting potential, in spite of the merely qualitative initial fit. Figures 1 and 2 show the fit, for representative energies, to the SG data with the

† Each of the eight terms in the potential had a basis of four harmonic oscillator functions, so that when SVD was not a limiting factor there were 32 parameters.

SG potential; $\chi^2/F = 5.84$ and $E_{\rm bound} = -1.611$ MeV. The J potential‡ fitted the J data equally well, $\chi^2/F = 5.95$ and $E_{\rm bound} = -1.8$ MeV. We comment below on the values of $E_{\rm bound}$. In both cases, the χ^2/F are calculated using uncertainties which do not represent all the errors discussed in the source references. In Figures 3 (Wigner terms) and 4 (Majorana terms) we compare the starting potential, i.e. the inversion potential for KKST MCRGM at 29.4 MeV, with the J and SG potentials. The (energy dependent) imaginary terms are evaluated at 8 MeV.

The J and SG potentials are very similar† and we compare them jointly with the RGM starting point. For the SG potential, the real, W, central potential had volume integral per nucleon pair $J_{\rm R} = 567.8$ MeV fm^3 and rms radius 3.01 fm; these values for potential J were 556.5 MeV fm^3 and 2.86 fm. If the energy dependence of Ref. [31] applies to $J_{\rm R}$ and to scattering from ^{4}He, the value at 30 MeV lab energy would be roughly 535 MeV fm^3, rather more than the RGM value of 499.72 MeV fm^3, (c.f. Section 4.1). The volume integral of the MCRGM real central W potential is thus a little less than the J and SG data, together with general deuteron scattering phenomenology, suggest. While it is true that D-state breakup would appreciably increase the depth over much of the radial range, the adiabatic model for 40 MeV suggests little modification to $J_{\rm R}$ due to the influence of repulsion in the far surface on the r^2 weighted integral for $J_{\rm R}$. Nevertheless, overall the RGM and empirical potentials are similar in shape. The most striking difference lies in the W, central, imaginary part; this is reasonable since the flux into inelastic channels must increase markedly between 8 and 29.4 MeV. The emissive region at the nuclear centre for this imaginary term is firmly established by inversion. This is not unusual in RGM inversion studies and there is a nearly emissive feature at the centre of the MCRGM potential, probably due to non-locality. There is nothing comparable in the unsymmetrised adiabatic breakup calculations. The W spin-orbit terms broadly follow the RGM shape. We have pointed out that the spin-orbit potential is not determined for $r < 0.5$ fm and the central cusps are probably an artifact of the harmonic oscillator basis. One curious feature is that fact that potential J has $J_{\rm R}$ which is slightly smaller in magnitude than that of potential SG. This is, of course, consistent with the higher mean energy of the data to which it is fitted, but the associated deeper binding for potential J is somewhat counter-intuitive. From another perspective it is not, perhaps, surprising that the potential (SG) which is constrained by data reaching to lower energies gives a better fit to the experimental binding energy, -1.472 MeV. However, the calculation of $J_{\rm R}$ and, even more the rms radius, demands that the potential be very well determined in the far surface; we cannot absolutely guarantee this at present.

Concerning the much smaller M terms in Figure 4: unsurprisingly, the J and SG potentials jointly differ more from the 29.4 MeV starting potential, and are probably poorly determined for $r < 1$ fm. The attractive real central term for $r > 1.5$ fm, where J and SG agree with RGM, seems to be well established.

These studies are continuing; the energy range will be increased, and the possibility that some irregular features in the potential are artefacts of an inadequate energy dependence and/or lack of tensor interaction studied.

‡ The fits shown during the oral presentation can be supplied by the author on request.
† The J potential discussed was determined by starting the inversion from SG potential; however, completely independent fitting led to a very similar potential.

5. Conclusions: what IP might do for the study of halo nuclei

Observable-to-potential IP inversion will find a local potential to fit any elastic scattering data. If data for several energies are available, so much the better, since continuity with energy is a useful criterion in evaluating ambiguities when what was otherwise impossible to fit precisely becomes all too easy to fit. In some cases, other *a priori* information can be incorporated.

IP inversion can contribute to a theoretical understanding of potentials. It readily yields local potentials corresponding to any theoretical model whatever; thus one can relate modifications to the model to changes induced in the potential. This opens the way to finding a rich variety of generic properties of the DPP or exchange contributions (especially for RGM), pointing to what is required to make good the difference between theoretical and empirical potentials.

Inversion for both experiment and theory for the same reaction makes local potentials of special value. The p + ^{4}He case discussed elsewhere, and the d + ^{4}He case discussed here show this. We have concluded that the KKST model gives a very good description of d + ^{4}He scattering even though the fits presented by KKST seem mediocre. For example, theory and data substantially agree the on the nature of the real Majorana terms; the imaginary Majorana terms probably require D-state breakup which we know is required in a complete description. A host of interesting theoretical puzzles arise from this work: for example, just how do non-locality effects lead to an emissive region at the nuclear centre rather than the deep absorptive region firmly predicated by unsymmetrised breakup calculations?

Acknowledgments

We are grateful to the EPSRC for grant GR/H00895 supporting Dr Cooper. We are particularly indebted to Professor V.I. Kukulin of Moscow for providing numerical data and much inspiration.

References

[1] S.G. Cooper, program IMAGO, unpublished; see also S.G. Cooper and R.S. Mackintosh, OU report OUPD9201
[2] K. Chadan and P.C. Sabatier, Inverse Problems in Quantum Scattering Theory, Second Edition, (Springer, New York, 1989)
[3] R.S. Mackintosh and A.M. Kobos, Phys. Lett. **116B** (1982) 95; A.A. Ioannides and R.S. Mackintosh, Nucl. Phys. **A438** (1982) 354.
[4] V.I. Kukulin, V.N. Pomerantsev and J. Horaček, Phys. Rev. **A 42** (1990) 2719
[5] V.I. Kukulin, V.N. Pomerantsev and S.B. Zuev, Yad. Fiz., **59** (1996) 428 ; English translation: Physics of Atomic Nuclei, **59** (1996) 403
[6] S.G. Cooper and R.S. Mackintosh, Phys. Rev. **C 43** (1991) 1001; Nucl. Phys. **A517** (1990) 285; Phys. Rev. **C 54** (1996) 3133
[7] S.G. Cooper, Nucl. Phys. **A 618** (1997) 82
[8] S.G. Cooper and R.S. Mackintosh, Inverse Problems, **5** (1989) 707
[9] S.G. Cooper and R.S. Mackintosh, Phys. Rev. **C54** (1996) 3133
[10] A.A. Ioannides and R.S. Mackintosh, Phys. Lett. **169B** (1986) 113
[11] R.S. Mackintosh and S.G. Cooper, J. Phys. G. **23** (1997) 565
[12] R.S. Mackintosh and S.G. Cooper, Nucl. Phys. **A589** (1995) 377
[13] S.G. Cooper and R.S. Mackintosh, Nucl. Phys. **A592** (1995) 338
[14] S.G. Cooper and R.S. Mackintosh, Nucl. Phys. **A576** (1994) 308
[15] M.A. McEwan, S.G. Cooper and R.S. Mackintosh, Nucl. Phys. **A552** (1993) 401
[16] S.G. Cooper and R.S. Mackintosh, Nucl. Phys. **A 582** (1995) 283

[17] M.C Mermaz, Phys. Rev. **C 47** (1993) 2213
[18] R.S. Mackintosh and S.G. Cooper, Nucl. Phys. **A625** (1997) 651, also preprint nucl-th/9708003.
[19] S.G. Cooper, Nucl. Phys. **A 626** (1997) 715, also preprint nucl-th/9708013.
[20] E.V. Kuznetsova and V.I. Kukulin, Yad. Fiz. **60** (1997) 608; English translation: Physics of Atomic Nuclei, **60** (1997) 528
[21] H. Kanada, T. Kaneko, S.Saito and Y.C. Tang, Nucl. Phys. **A444** (1985) 209
[22] M. LeMere, Y.C. Tang and D.R. Thompson Nucl. Phys. **A266** (1976) 1
[23] M. Yahiro, M. Nakano, Y.Ieri and M. Kamimura, Prog. Theor. Phys. **67** (1982) 1038; H. Amakawa, A. Mori, H. Nishioka, K. Yazaki and S. Yamaji, Phys. Rev. **C 23** (1981) 583; I.J. Thompson and M. Nagarajan, Phys. Lett. **106B** (1981) 163
[24] I.J. Thompson, code Adia, private communication from J. Tostevin.
[25] V.I. Kukulin, V.N. Pomerantsev, S.G. Cooper and S.B. Dubovichenko, preprint nucl-th/9711034
[26] E.V. Kuznetsova and V.I. Kukulin, Physics of Atomic Nuclei **60** (1997) 528 (Translation of Yad. Fiz. **60** (1997) 608)
[27] S.G. Cooper, V.I. Kukulin, R.S. Mackintosh and E.V. Kuznetsova, in preparation
[28] B. Jenny, W. Gruebler, V. König, P.A. Schmelzbach, and C. Schwizer, Nucl. Phys. **A397** (1983) 61.
[29] L.S. Senhouse and T.A. Tombrello, Nucl. Phys. **57** (1964) 624
[30] W. Gruebler, P.A. Schmelzbach, V. König, and P. Marmier, Nucl. Phys. **A 134** (1969) 686
[31] C.M. Perey and F.G. Perey, Phys. Rev. **132** (1963) 755

Figure captions

Figure 1. For deuterons scattering from ^{4}He, the differential cross-sections calculated with potential SG compared with data measured at 6 energies in the range from 2.93 MeV and 11.475 MeV as measured by Senhouse and Tombrello. Potential SG was determined as described in the text by fitting differential cross-sections for all 19 energies and analysing power for 12 energies.

Figure 2. For deuterons scattering from ^{4}He the vector analysing powers calculated with potential SG compared with data measured at 6 energies in the range from 3.00 MeV and 11.0 MeV measured by Gruebler *et al*. Potential SG was determined as described in the text by fitting analysing powers for all 12 energies and cross-sections for 19 energies.

Figure 3. The Wigner (W) components of the starting potential (fitting KKST S_{lj}) and potentials J and SG. From the top we present the real and imaginary central, then real and imaginary spin-orbit components. The solid line is the KKST fit for 29.4 MeV lab, the dashed line is potential SG and the dotted line is potential J.

Figure 4. The Majorana (M) components of the same potentials as in the previous figure, with the same order and same conventions.

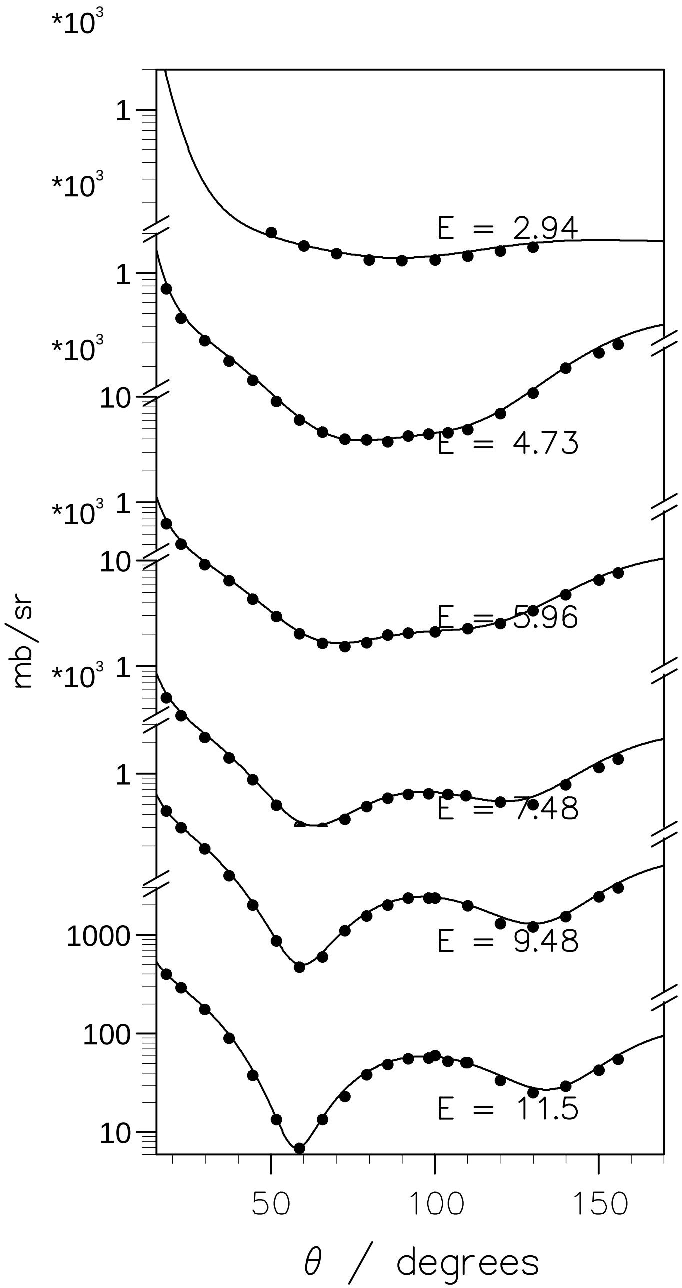

*10^3
1
*10^3
E = 2.94
1
*10^3
10
E = 4.73
1
*10^3
10
E = 5.96
1
*10^3
1
E = 7.48
1000
E = 9.48
100
E = 11.5
10
mb/sr
50
100
150
θ / degrees

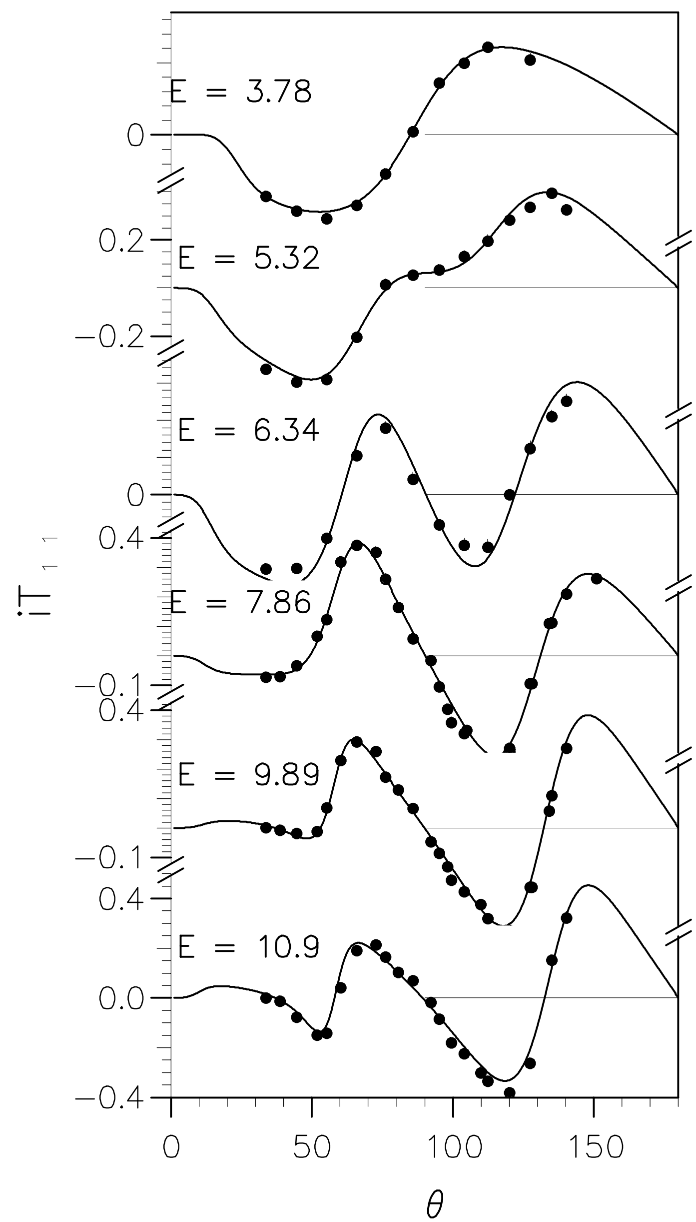
E = 3.78
E = 5.32
E = 6.34
E = 7.86
E = 9.89
E = 10.9
0
0.2
−0.2
0
0.4
−0.1
0.4
−0.1
0.4
0.0
−0.4
0
50
100
150
iT_{11}
θ

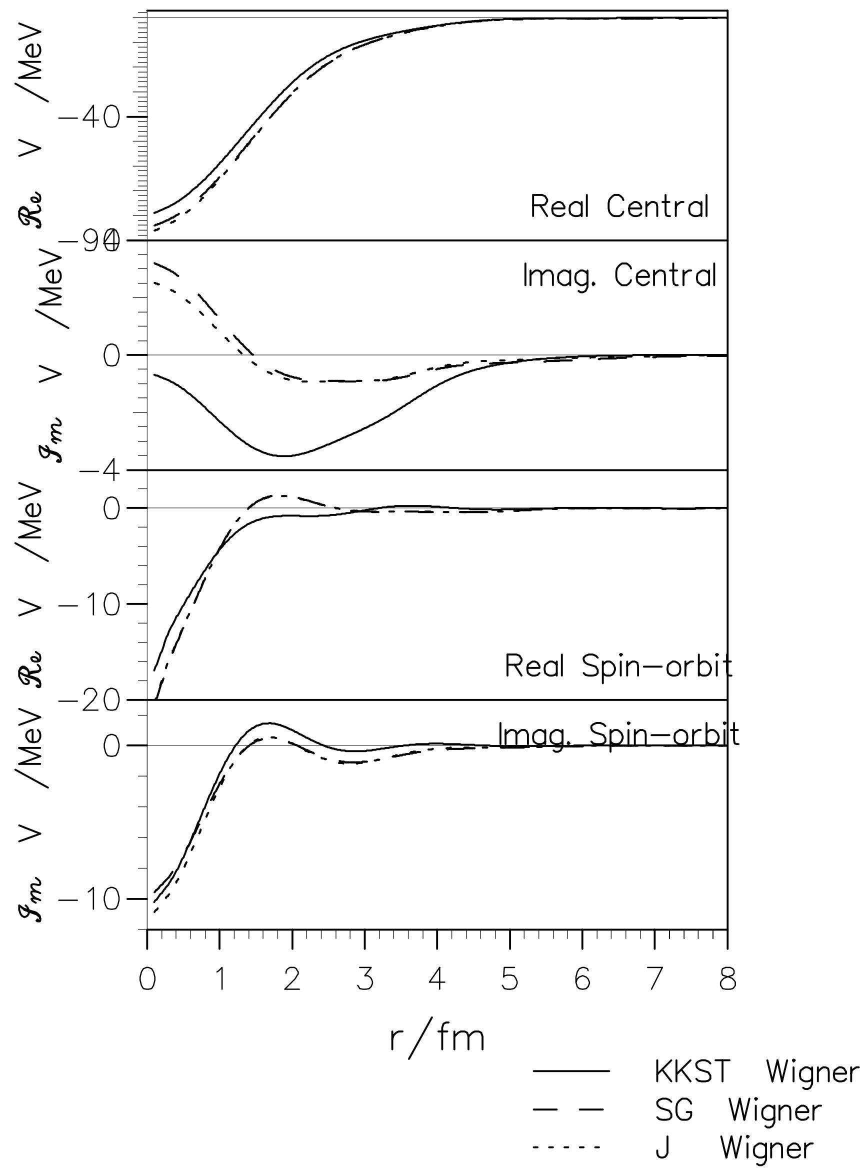

Real Central
Imag. Central
Real Spin−orbit
Imag. Spin−orbit
ℛe V /MeV
ℐm V /MeV
−40
−90
4
0
−4
−10
−20
0 1 2 3 4 5 6 7 8
r/fm
KKST Wigner
SG Wigner
J Wigner

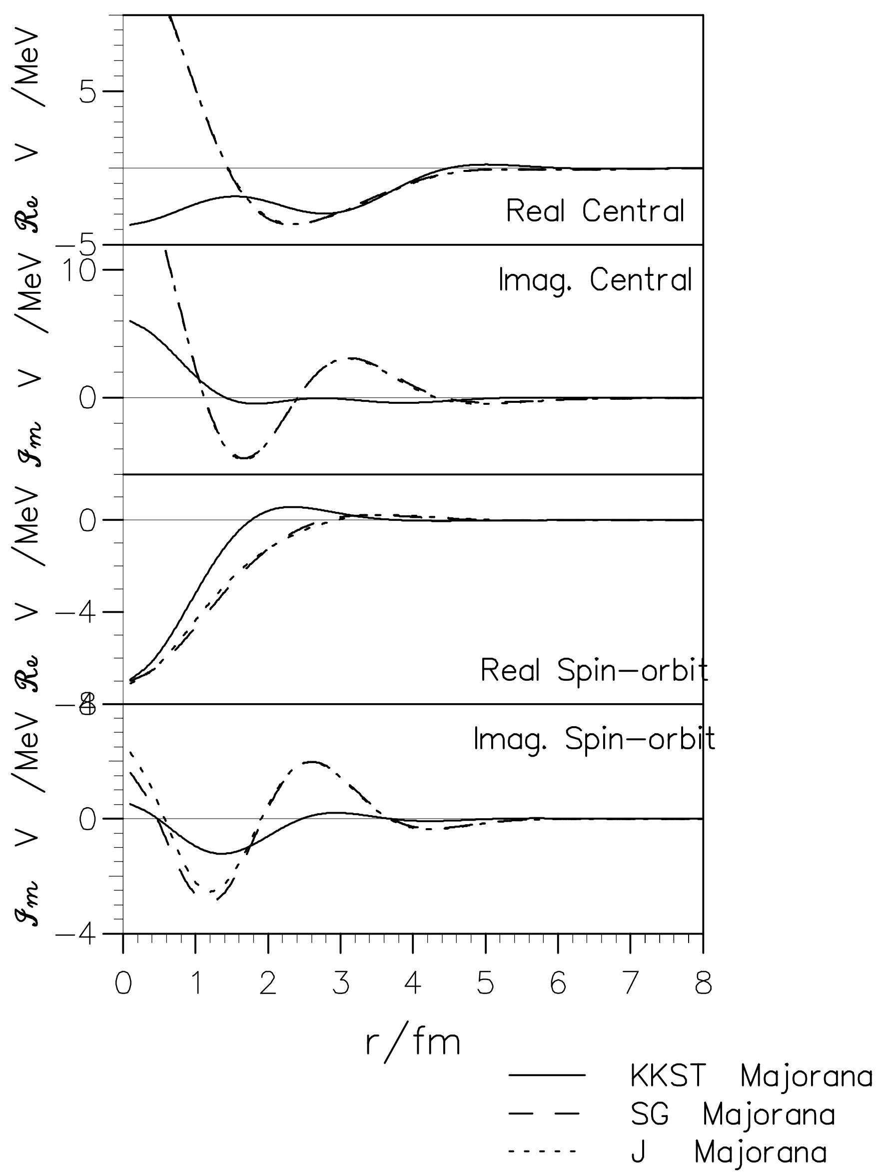

Real Central
Imag. Central
Real Spin–orbit
Imag. Spin–orbit
$\mathcal{Re}$ V /MeV
$\mathcal{Im}$ V /MeV
r/fm
KKST Majorana
SG Majorana
J Majorana